On the local charge inhomogeneity and lithium distribution in the superionic argyrodites Li_6PS_5X (X = Cl, Br, I)

Nicolò Minafra[a,b], Marvin A. Kraft[a,b], Tim Bernges[a,b], Cheng Li[c], Roman Schlem[a,b], Benjamin J. Morgan[d], Wolfgang G. Zeier*[a,b]

[a]*Institute of Physical Chemistry, Justus-Liebig-University Giessen, Heinrich-Buff-Ring 17, D-35392 Giessen, Germany.*

[b]*Center for Materials Research (LaMa), Justus-Liebig-University Giessen, Heinrich-Buff-Ring 16, D-35392 Giessen, Germany.*

[c]*Jülich Centre for Neutron Science (JCNS), Forschungszentrum Jülich GmbH, Outstation at SNS, 1 Bethel Valley Road, Oak Ridge, Tennessee 37831-6473, United States*

[d]*Department of Chemistry, University of Bath, Claverton Down BA2 7AY, United Kingdom*

Abstract

The lithium-argyrodites Li_6PS_5X (X = Cl, Br, I) exhibit high lithium-ion conductivities, making them promising candidates for use in solid-state batteries. These solid electrolytes can show considerable substitutional X^-/S^{2-} anion-disorder, typically correlated with higher lithium-ion conductivities. The atomic-scale effects of this anion site-disorder within the host lattice—in particular how lattice disorder modulates the lithium substructure—are not well understood. Here, we characterize the lithium substructure in Li_6PS_5X (X = Cl, Br, I) as a function of temperature and anion site-disorder, using Rietveld refinements against temperature-dependent neutron diffraction data. Analysis of these high-resolution diffraction data reveals an additional lithium position previously unreported for Li_6PS_5X argyrodites, suggesting that the lithium conduction pathway in these materials differs from the most common model proposed in earlier studies. Analysis of the Li^+ positions and their radial distributions reveals that greater inhomogeneity of the local anionic charge, due to X^-/S^{2-} site-disorder, is associated with more spatially-diffuse lithium distributions. This observed coupling of site-disorder and lithium distribution provides a possible explanation for the enhanced lithium transport in anion-disordered lithium argyrodites, and highlights the complex interplay between anion configuration and lithium substructure in this family of superionic conductors.

1. Introduction

Inorganic solid-state ionic conductors have the potential to be used as electrolytes for all-solid-state batteries; which, compared to conventional lithium-ion batteries, are expected to offer improved device safety as well as increased energy and power densities.[1–4] The lithium-argyrodites Li_6PS_5X (X = Cl, Br, I) have attracted considerable attention in this regard, due to their high ionic conductivities, reasonable electrochemical stabilities, and negligible grain boundary resistances.[5–16] The argyrodites take their name from the naturally occurring mineral Ag_8GeS_6, which possess highly mobile Ag^+ ions.[17–23] The synthetic Li_6PS_5X lithium-argyrodites are derived by replacing silver with lithium and substituting one chalcogen per formula unit with a halide ion. A large number of lithium-argyrodite compositions have previously been synthesized,[24–31] with some of the highest room temperature ionic conductivities reported for the $Li_{6+x}P_{1-x}Ge_xS_5I$ and $Li_{6+x}Sb_{1-x}Si_xS_5I$ series.[32,33]

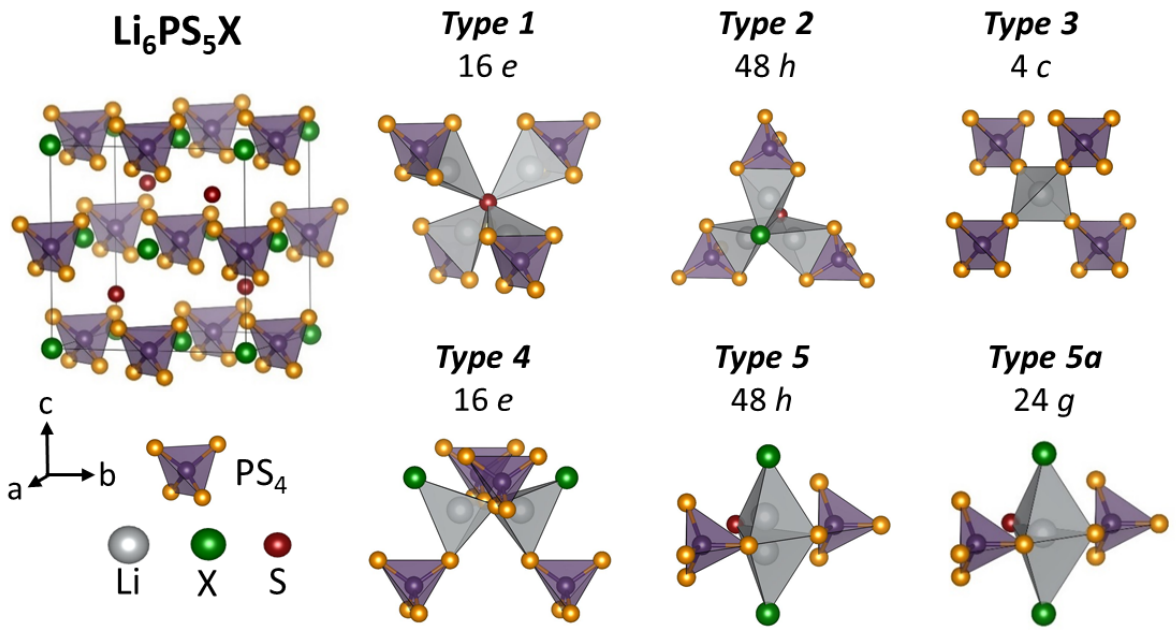

Figure 1: Unit cell of Li_6PS_5X (X = Cl, Br, I), with panels showing the local coordination of the five types of tetrahedral interstitial sites, alongside the trigonal coordinated type 5a site. This classification follows the nomenclature proposed by Deiseroth et al. with symmetry labels referring to the inverted setting 2.[34] In line with this notation, the X^- anions occupy Wyckoff 4a positions, while S^{2-} ions Wyckoff 4d. P and S part of the PS_4^{3-} units reside on Wyckoff 4b and 16e, respectively.

Lithium-argyrodites exhibit both low- and high-temperature polymorphs, with phase transition temperatures that strongly depend on their specific composition.[34,35] The highly conductive,

high temperature polymorph is based on a tetrahedrally close-packed anion lattice in the cubic $F\bar{4}3m$ space group (Figure 1). In the conventional anion-ordered Li_6PS_5X structure the X^- anions (Wyckoff 4*a*) form a cubic–close-packed lattice. PS_4^{3-} units occupy the octahedral sites (P and S on Wyckoff 4*b* and 16*e*, respectively) and S^{2-} ions occupy one half of the tetrahedral holes (Wyckoff 4*d*). Li_6PS_5I typically adopts this anion-ordered structure, with the X^- and S^{2-} anions occupying distinct crystallographic sites. Li_6PS_5Br and Li_6PS_5Cl, however, typically adopt anion-disordered structures, in which the X^- and S^{2-} anions are significantly disordered across the Wyckoff 4*a* and 4*d* sites,[9,17] with the precise degree of anion-disorder tunable by adjusting synthesis protocols.[36] The origin of this anion–site-disorder has not been unequivocally resolved, but theoretical and experimental analyses suggest that anion mixing is facilitated by the similar ionic radii for S^{2-} versus Br^- or Cl^-.[9,37] The absence or presence of site-disorder in Li_6PS_5X argyrodites strongly affects their lithium transport properties. Li_6PS_5I (anion-ordered) is a poor Li-ion conductor compared to Li_6PS_5Cl and Li_6PS_5Br (both anion-disordered), which exhibit $\times 10^3$ higher room-temperature ionic conductivities.[9,13,38–40]

While the correlation between anion disorder and fast lithium transport is well documented,[9,24–33,36,41] the effect of anion site-disorder on the microscopic dynamics and local structure of the mobile lithium ions is less well understood. In Li_6PS_5X argyrodites, the anionic framework contains 132 tetrahedral voids per unit cell (4 formula units) that may accommodate the corresponding 24 lithium ions. The 132 tetrahedral interstices can be classified into five types (Figure 1), based on the number of corners or edges each tetrahedron shares with neighboring rigid PS_4^{3-} units.[34,42] Previous neutron diffraction studies of Li_6PS_5X have assigned lithium ions as only occupying type 5 sites (Wyckoff 48*h*), with observations of a "smeared out" lithium density usually interpreted as some lithium occupying an additional "site", here denoted as type 5a (Wyckoff 24*g*), located at the shared face of adjacent type 5 tetrahedra pairs.[9,34] The type 5 and type 5a sites together form cage-like geometries, centered around the nominal S^{2-} positions on Wyckoff 4*d* (Figure 4b).

The conventional model for lithium diffusion in Li_6PS_5X argyrodites considers lithium motion only in terms of "jumps" between the type 5 and 5a sites, with jumps usually classified into three types.[39] *Doublet* jumps represent localized motion between face-sharing type 5 tetrahedra, via the type 5a site. *Intra*-cage jumps consist of lithium motion between pairs of non-face-sharing type 5 tetrahedra within the same 4*d*-centered cage. *Inter*-cage jumps consist of lithium motion between type 5 positions associated with *different* 4*d*-centered Li^+ cages. Within this three-jump model, long-ranged lithium diffusion throughout the argyrodite lattice is viable only if all three classes of jumps occur.[39]

This three-jump model, in which the lithium diffusion mechanism is described entirely in terms of movement between type 5 sites, has been widely applied to explain experimental and theoretical trends in lithium transport in Li_6PS_5X and related lithium-argyrodites.[9,24–32,41,43] This model, however, ignores the role of non-type 5 tetrahedra, and therefore gives an incomplete description of the lithium diffusion pathways in the argyrodite structure. The type 5 tetrahedra form face-sharing pairs, and pure 5 → 5 lithium motion is only possible for the *doublet* jump. Longer-ranged lithium motion, *i.e.* between non-face-sharing type 5 tetrahedra, requires lithium ions to pass through non-type 5 tetrahedra.[38,42] The role of non-type 5 tetrahedral sites in any contiguous lithium-diffusion pathways through the argyrodite lattice has previously been highlighted by analysis of bond valence calculations,[40,44,45] and molecular dynamics simulations.[42,46] Lithium occupation of non-type 5 sites has also been experimentally observed in "Li-excess" argyrodites with lithium stoichiometries $x(\mathrm{Li}) > 6$,[33,47,48] such as $Li_{6+x}Sb_{1-x}Si_xS_5I$ together with the halide-free compositions $Li_{6.15}M'_{1.5}S_6$ and the related oxysulfides $Li_{6.15}M'_{1.5}S_{5.4}O_{0.6}$ ($M' = Al_{0.1}Si_{0.9}$), and it has been proposed that occupation of non-type 5 sites is a direct consequence of these $x(\mathrm{Li}) > 6$ stoichiometries.[33] Furthermore, Li-excess systems, such as $Li_{6+x}P_{1-x}Ge_xS_5I$ and $Li_{6+x}Sb_{1-x}Si_xS_5I$, exhibit some of the highest reported room-temperature ionic conductivities within the lithium-argyrodite family.[32,33] The correlation between this unusual lithium-site occupation and high ionic conductivities has prompted the suggestion of a causal link, whereby partial occupation of non-type 5 sites promotes fast, highly concerted lithium diffusion, making the redistribution of lithium the origin of these systems' exceptional ionic conductivities.[33]

This idea, that in the lithium argyrodites the distribution of lithium over interstitial sites is qualitatively different for systems with lithium stoichiometries $x(\mathrm{Li}) = 6$ versus $x(\mathrm{Li}) > 6$, and that this difference explains the exceptional ionic conductivities of the Li-excess $x(\mathrm{Li}) > 6$ systems, depends on a structural model of $x(\mathrm{Li}) = 6$ Li_6PS_5X systems in which only type 5 (and 5a) sites are occupied. While this model is consistent with previous neutron diffraction analyses,[9,24-27,32–35,40] recent first principles molecular dynamics simulations of Li_6PS_5X (X = I, Cl) have predicted that non-type 5 sites may be significantly occupied even for these $x(\mathrm{Li}) = 6$ systems.[42] These simulations also predict that the proportion of lithium occupying non-type 5 sites increases with the degree of X^-/S^{2-} site exchange, while the relationship between the proportion of lithium occupying non-type 5 sites and lithium diffusion is more complex: systems with 100 % X^-/S^{2-} site-inversion exhibited the highest proportion of lithium in non-type 5 sites, but had poor lithium diffusion comparable to fully-ordered Li_6PS_5X.[42]

Motivated by apparent contradiction between this theoretical study and existing experimental data, and to better understand the relationships between chemical composition, degree of site disorder, and lithium distribution, we have performed an experimental analysis of the lithium substructure in the Li_6PS_5X (X = Cl, Br, I) lithium argyrodites. To monitor the subtle changes of the lithium substructure with temperature, we have conducted high-resolution, temperature-dependent neutron powder diffraction measurements. In anion-ordered Li_6PS_5I we assign lithium as exclusively occupying the type 5 and 5a sites, while in anion-disordered Li_6PS_5Br and Li_6PS_5Cl we identify a considerable fraction of lithium ions located at type 2 sites, in agreement with the recent theoretical predictions.[42] Analysis of the lithium radial distributions reveals that anion site-disorder, which can be considered as introducing anionic charge inhomogeneity, is correlated with a more spatially-diffuse lithium distribution. We note that this more delocalized lithium density is therefore correlated with the enhanced lithium transport properties observed for the anion-disordered Li_6PS_5Br and Li_6PS_5Cl, suggesting a possible mechanistic link between anion disorder and high lithium conductivities in these materials.[42] The observation of such differences in the lithium substructure between anion-ordered and anion-disordered argyrodites, and the confirmation that a large fraction of lithium can reside on non-type 5 sites even for x(Li) = 6 stoichiometries highlights the importance of considering these additional sites in mechanistic models of lithium diffusion in lithium argyrodites, and more generally suggests the need for a reevaluation of structure–transport correlations in this family of solid electrolytes.

2. Experimental Section

Synthesis. Li_6PS_5X (X = Cl, Br, I) samples were prepared via high temperature solid-state reaction. Lithium sulfide (Li_2S, Alfa-Aesar, 99.9%), phosphorus pentasulfide (P_4S_{10}, Merck, 99%), and the lithium halide (LiCl, LiBr and LiI, ultradry Alfa-Aesar, 99.99%) were mixed in the appropriate stoichiometric ratio and hand-ground in an agate mortar for 15 min. The obtained mixtures were pelletized and then filled into quartz ampoules, which were sealed under vacuum. Prior to the filling, the quartz tubes were carbon coated and preheated at 800 °C under dynamic vacuum to remove all trace of water in the reaction atmosphere. The reactions were performed at 550 °C for 2 weeks (100 °C h^{-1} heating rate and natural cooling) to achieve phase purity. After annealing, the obtained products were ground and used for the diffraction studies.

Neutron powder diffraction. Neutron powder diffraction data were collected at Oak Ridge spallation neutron source (SNS, Oak Ridge National Laboratory) using the JANIS cryo-furnace at POWGEN diffractometer (BM11-A beamline).[49–51] Approximately 3 g of sample were

loaded into a 8 mm diameter cylindrical vanadium can under an inert atmosphere and sealed with a copper gasket to avoid air exposure during measurements. Using a single bank with center wavelength of 1.5 Å, data were collected in high-resolution mode from 150 K to 350 K every 50 K for approximately 2 h. This bank allowed to probe a *d*-spacing range from 0.5 up to 6 Å with a resolution $\delta d/d < 9 \cdot 10^{-3}$.[51] The obtained diffractograms are shown in the Supporting Information, Figure S1–S3

Rietveld analysis. Rietveld refinements were carried out using TOPAS-Academic V6 software package.[52] The structural data obtained from neutron refinements of Li_6PS_5X from Kraft *et al*.[9] were used as starting model. The peak profile shape was described by a convolution of pseudo-Voigt and GSAS back-back exponential function. Fit indicators – R_{wp}, and Goodness-of-fit (GoF) were used to assess the quality of the refined structural model. The following parameters were initially refined: (1) scale factor (2) background (10 coefficients Chebyshev function), (3) peak shape and (4) lattice parameters. After a suitable fit of the profile was achieved, the structural parameters were allowed to refine. Initially, (5) fractional atomic coordinates, (6) isotropic atomic displacement parameters and (7) atomic occupancies were refined. Finally, lithium occupancy on other possible interstitial sites was investigated. The coordinates of these voids are tabulated in the Supporting Information, Table S1. The occupancy on these sites was constrained to the occupancy of the lithium positions proposed by Kraft *et al.*[9] to maintain the nominal stoichiometry and charge neutrality. Output lithium atomic displacement parameters were used as indicators for probing the authenticity of the eventual occupancy, where unphysical or negative values suggest the absence of lithium in the probed sites. The stability of the refinements was ensured by allowing to refine multiple correlated parameters simultaneously over several cycles. The refinements at different temperatures were performed in a sequential mode and the consistency of the obtained structural models was corroborated by utilizing different starting parameters. Finally, the crystallographic information files reported in the Supporting Information were obtained by allowing to refine all possible structural parameters at the same time, further proving the stability of the refined structure. The constraints applied during Rietveld refinements are also tabulated in the Supporting Information, Table S2–S4.

3. Results

Topological analysis of the connectivity between tetrahedral interstices within the argyrodite lattice,[38,42] as well as experimental data for $Li_{6+x}Sb_{1-x}M_xS_5I$ (M = Si, Ge), $Li_{6.15}M'_{1.5}S_6$ and the

related oxysulfide $Li_{6.15}M'_{1.5}S_{5.4}O_{0.6}$ (M' = $Al_{0.1}Si_{0.9}$),[33,47,48] and the recent theoretical predictions for Li_6PS_5X (X = I, Cl),[42] all highlight the possible occupation of non-type 5 sites in the Li_6PS_5X lithium argyrodites. While these non-type 5 sites must play a role in long-ranged Li diffusion in all argyrodites, to our knowledge, no previous experimental evidence exists for non-negligible occupation in Li_6PS_5X (X= Cl, Br, I). Although a number of neutron diffraction studies on this class of materials have already been reported,[9,24–27,32–35,40] the availability of new high-resolution time-of-flight neutron powder diffractometers[51] encourages a re-evaluation of the lithium substructure in these materials. Due to the fast–ion-conducting nature of Li_6PS_5X, low-temperature measurements are required to "freeze-in" the motion of the Li^+ ions, so that otherwise hidden lithium positions may be observed, and to allow subtle changes in the lithium sublattice to be resolved. At low temperatures lithium ions may stabilize in sites along diffusion pathways without being significantly perturbed by the thermal displacement of the surrounding sites. The temperature-dependence of the lithium distribution also helps provide insight into the underlying potential energy surface that dictates the viability of competing lithium diffusion pathways. To revisit the lithium substructure of the lithium argyrodites Li_6PS_5X (X = Cl, Br and I), therefore, we have characterized the lithium distribution in these materials using high resolution neutron diffraction data collected in the temperature range of 150 K – 350 K.

Exemplary Rietveld refinements of the neutron diffraction data for Li_6PS_5X (X = Cl, Br, I) at 200 K are shown in Figure 2, with a close up of the lower d-spacing range showing the good agreement of the calculated diffraction pattern with the experimental data. In addition, all obtained diffractograms are shown in the Supporting Information, Figure S1–S3. Within the studied temperature range, the diffractograms can be well described by the cubic high temperature structure, crystallizing in the $F\bar{4}3m$ space group, with the exception of Li_6PS_5I that undergoes a phase transition to the low temperature polymorph below 200 K.[34] All constraints used for the refinements and the crystallographic information files can be found in the Supporting Information, Tables S2–S4.

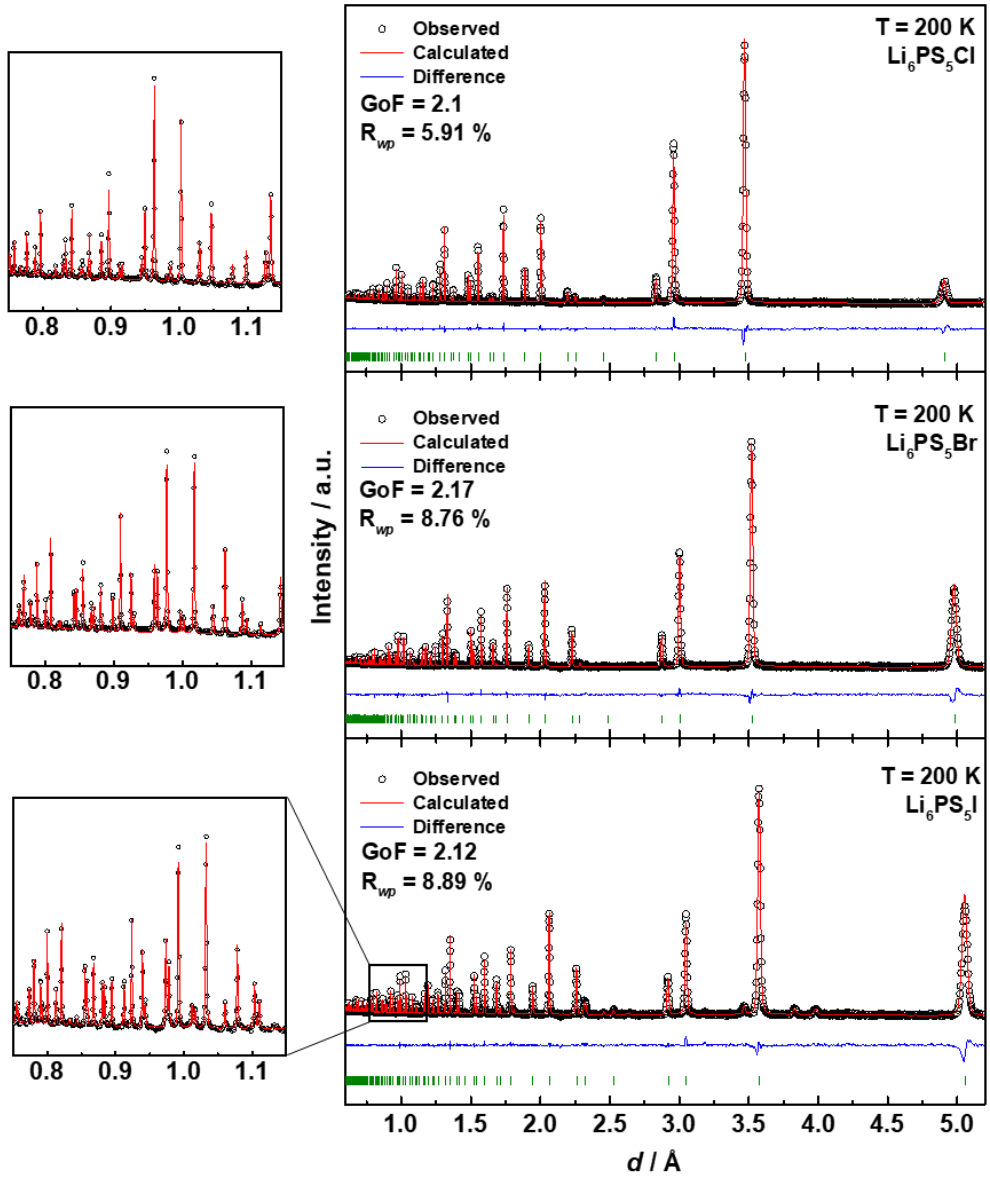

Figure 2: Exemplary Rietveld refinements against neutron powder diffraction data measured at 200 K relative to Li_6PS_5X (X = Cl, Br and I). Experimental data are shown in black and the red line denotes the calculated pattern, whereas the difference profile is shown in blue. Positions of the Bragg reflections are shown as green vertical ticks. The low values for the fit indicators together with matching intensity at lower d-spacing (inserts) confirm the good quality of the calculated structural model.

Expanding lattices. Figure 3a shows the obtained lattice parameters of Li_6PS_5X (X = Cl, Br, I) in the studied temperature range. The extracted room temperature lattice parameters are in line with the literature values, in which the ionic radii of the halides, $r_{Cl} < r_{Br} < r_{I,}$ dictate the different sizes of the unit cells.[9,34,53] Further, the lattice parameters increase linearly with temperature showing a similar positive thermal expansion behavior. Besides changes in the lattice volume,

the different ionic radii of the halides correlate with different degrees of site-disorder between the nominal free sulfur S^{2-} (*i.e.* not part of the PS_4^{3-} units) and the halide positions (Wyckoff 4*d* and 4*a*, respectively). The occurrence of site-disorder and its influence on the ionic transport has been intensively investigated experimentally and computationally.[9,24–28,32,41,43] The here-obtained X^-/S^{2-} site-disorder is quantified in Figure 3b. In agreement with the literature, a higher degree of disorder can be found for the chloride compared to the bromide counterpart, which can be attributed to the similar ionic radii of S^{2-} and Cl^-,[9,25,29] compared to the more dissimilar radii of S^{2-} and Br^-,[9,24,27,36] while no site-disorder is observed for Li_6PS_5I.[9,17,34] The extent of the site-disorder does not change with temperature, indicating that within this modifications to the degree of disorder due to changing the temperature treatment are not occurring within our investigated temperature-range.[36]

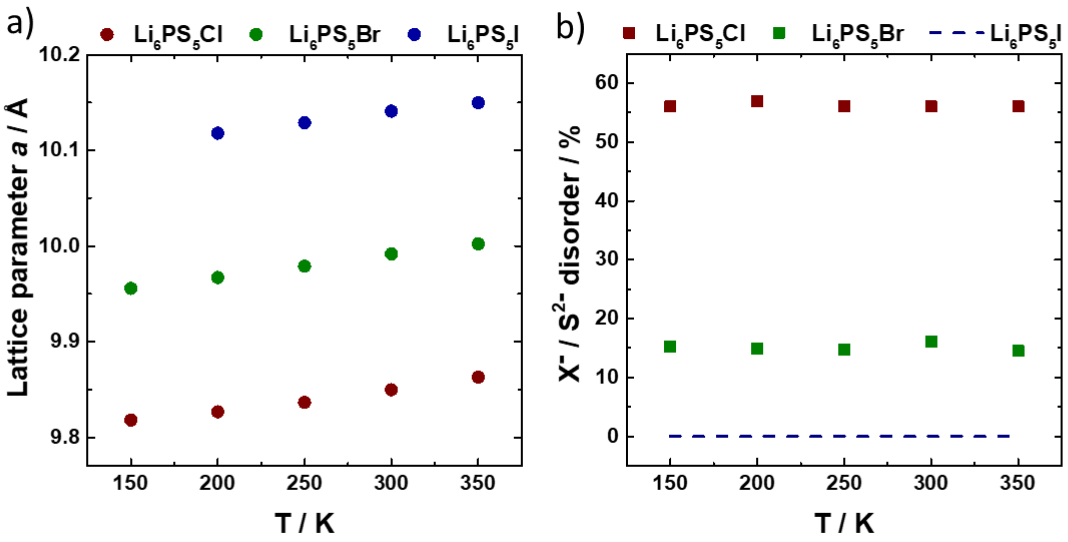

Figure 3: (a) The lattice parameters of Li_6PS_5X (X = Cl, Br, I) increase with increasing ionic radii of the halide anions and with temperature. Li_6PS_5I undergoes a phase transition to the low temperature polymorph below 200 K and is hence not shown here. (b) Site-disorder between halide and sulfur anions, which decreases with increasing anion radius (i.e. increasing X^-/S^{2-} size mismatch) and remain constant along the explored temperature range. The obtained refinement uncertainties, not shown, are smaller than the symbols.

Lithium substructure and occupation of non-type 5 Li^+ sites. To investigate the differences in the lithium sublattice as a function of *X* = Cl, Br, I and temperature, the possible lithium occupancies on the different available lithium sites in the structure need to be probed. Within the argyrodite structure, the tetrahedrally close-packed anion sublattice contains six symmetry inequivalent types of tetrahedral interstices, with five of these available to potentially

accommodate lithium. These tetrahedra can be classified as types 1–5 based on the numbers of common corners, edges, or faces shared with adjacent PS_4^{3-} units, and are considered here together with one additional trigonal-coordination position (Figure 1).

Starting from the typical structural model,[9] which only includes the type 5 (T5) and type 5a (T5a) sites, usually referred to as 48*h* and 24*g*, respectively, lithium occupancies were refined on all possible available tetrahedral voids in the structure. The coordinates of these voids are tabulated in the Supporting Information, Table S1. Whenever the refinements resulted in unphysical cation–anion distances or unphysically negative thermal displacement parameters and occupancies, the site was disregarded as not exhibiting lithium occupancy. Figure 4a shows the found occupancies of the various Li^+ sites in Li_6PS_5X (X = Cl, Br, I) as a function of temperature. In the case of Li_6PS_5I, no other suitable Li^+ positions were assigned besides the two T5 and T5a sites commonly reported in the literature.[9,40] In contrast, for X = Cl and Br, in addition to the positions already known from literature,[9,40] partial lithium occupancy is also found at the type 2 (T2) site. Figure 4b and c show the disconnected "cage" geometry of the typically reported type 5 and 5a positions and the improved connectivity of the lithium network when type 2 sites are included, respectively. Exemplary Fourier maps for Li_6PS_5Cl can be found in the Supporting Information, Figure S4, showing the need to include a T2 site. When averaging over the explored temperature range, 28 % and 16 % of the total lithium in the unit cell occupies the T2 site for X = Br and Cl, respectively. Lithium occupancy on the T2 site was previously suggested for $Li_{6+x}Sb_{1-x}Si_xS_5I$,[33] with this additional occupancy on T2 suggested to stem from the x(Li) > 6 lithium stoichiometry. Our result here shows that even in structures with a nominal composition of Li_6PS_5X (X = Cl, Br) a significant proportion of lithium ions can occupy the previously unexplored T2 site. We note that the atomic displacement parameter of lithium on the T2 site in Li_6PS_5Br is large (B_{eq} > 14 Å^2) to be of real physical meaning, suggesting a complex lithium-ion potential energy landscape, even at low temperatures. In addition to the T2 site found occupied here, previous molecular dynamics simulations have predicted partial lithium occupation of type 4 sites,[42] that cannot be experimentally confirmed within the here-probed compositions and temperature range.

Looking more closely at the changes of the lithium population on these sites with the temperature (Figure 4a), we find that the occupancy on type 5 sites always decreases with increasing temperature, while the occupancy on type 2 and 5a increases. This trend suggests that the type 5 sites correspond to low energy positions, while the type 2 and 5a sites correspond to higher energy positions, with occupation of these latter sites possibly promoted by entropic contributions at higher temperatures. The observation that increasing temperature causes a

greater proportion of lithium ions to occupy these "higher energy" sites is consistent with the recent proposal that T2 sites might play a critical role in lithium diffusion across the Li-argyrodite family.[38,40,42]

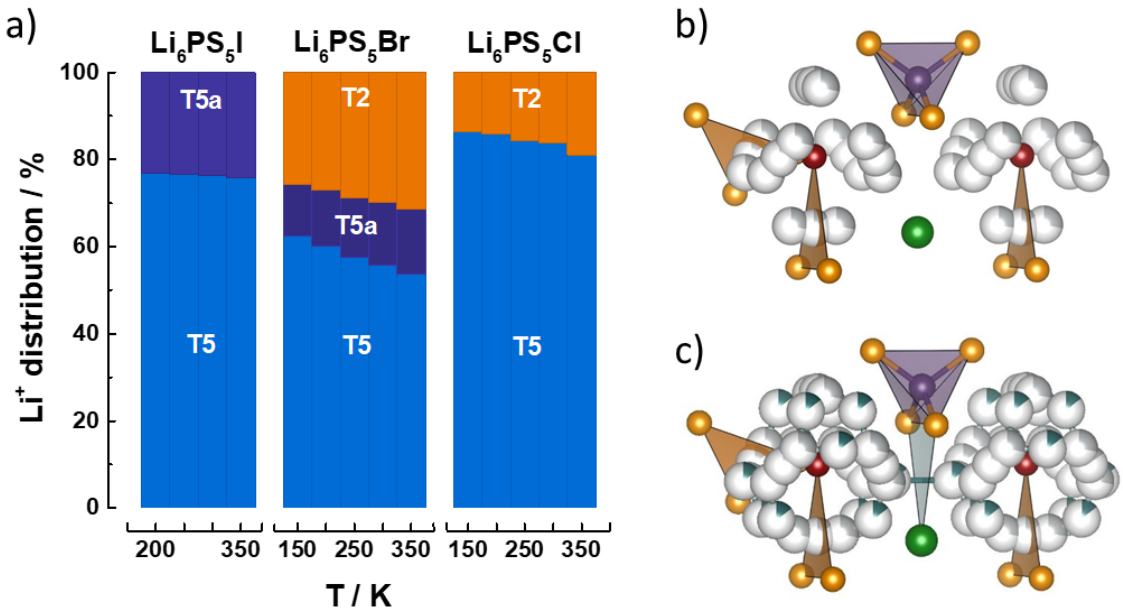

Figure 4: a) As assigned lithium distribution for Li_6PS_5X on the T5, T5a, and T2 sites, as a function of temperature. For all three compositions, the lithium occupancies decrease for type 5 positions, while it increases for type 2 and 5a with temperature, indicating the importance of the type 2 sites for the diffusion process. Panel (b) shows the disconnected "cage" geometry of the typically reported type 5 and 5a positions (gray), while panel (c) illustrates the improved connectivity of the lithium diffusion network when type 2 sites (tail) are included.

To obtain a better understanding of how the site-disorder between X^- and S^{2-} affects the lithium distribution, Figure 5 compares a radial distribution of Li^+ distances from the nominal free sulfur position (Wyckoff 4*d*) as a function of the changing halide anions. The radial distribution of the Li^+ is calculated as number of lithium ions located on each specific site in one cage (*i.e.* T2, T5 or T5a) multiplied by the occupancy obtained via the Rietveld refinement, plotted as a function of the distance from the central X^-/S^{2-} anion (Wyckoff 4*d*). It is important to note that this analysis gives an averaged lithium distribution that does not capture any local positional disorder the lithium sites might exhibit; for example, as a result of different numbers of S^{2-} and X^- anions sitting at the vertices of otherwise equivalent tetrahedral sites in the anion-disordered systems.[42] To obtain better visual resolution, in Figure 5 we superimpose data obtained for all explored temperatures. While we do observe changes in the lithium positions with temperature, this effect is small when compared with the differences in the distance between lithium and the

different anionic centers in Li_6PS_5X as a function of X^-. From our Li^+ radial distribution analysis, we observe that the lithium cations are the smallest distance from the anion at the center of the cage (Wyckoff 4*d* position) for Li_6PS_5I, with this distance increasing for Li_6PS_5Br and more-so for Li_6PS_5Cl. This shows that although the lattice volume increases in the series $Li_6PS_5Cl \rightarrow Li_6PS_5Br \rightarrow Li_6PS_5I$ the distribution of lithium around the Wyckoff 4*d* sites is most contracted for Li_6PS_5I. This trend can be understood by considering that Li_6PS_5I exhibits no site-disorder and only S^{2-} can be found in the center of the 4*d*-centered cages, representing the highest negative charge density located inside these cages (Figure 5). Li_6PS_5Br exhibits a moderate degree of disorder with 15 % site-inversion, while Li_6PS_5Cl shows significantly more disorder with 56 % Cl^- located at the center of these Li^+ cages, giving the lowest magnitude average 4*d*-site charge. Figure 6a shows the average distance r_{mean} of the Li^+ away from the center of the 4*d*-cage (weighted by the respective lithium occupancies) plotted against the degree of site-disorder for each of the three systems. Higher site-disorder corresponds to a lower average anionic charge density in the center of the cage, as S^{2-} is progressively replaced with X^-. This produces a weaker bonding environment for the lithium within the cage giving longer average Wyckoff 4*d*–Li distances and shorter average distances to the nominal halide 4*a* position (Figure 6b). While the results obtained from the diffraction analysis can only capture a spatial average of the lithium configuration, these results are broadly in line with data obtained from previous molecular dynamics simulations.[42]

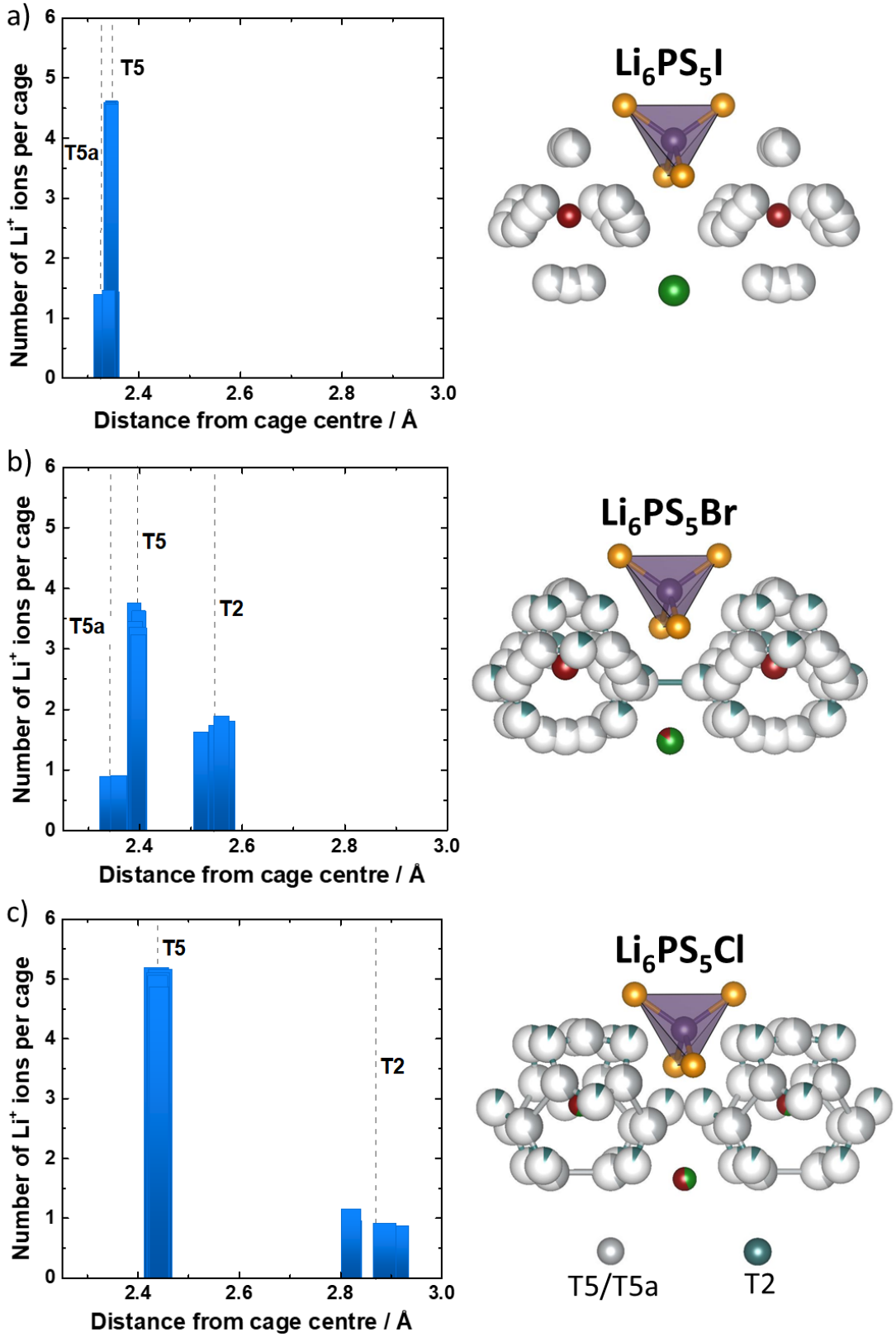

Figure 5: Radial distribution of Li^+ around the center anion X^-/S^{2-} (Wyckoff 4d) in the lithium cage for all temperatures, along with the lithium positions for (a) Li_6PS_5I, (b) Li_6PS_5Br and (c) Li_6PS_5Cl at 200 K. The radial distribution shows an increasing Li^+ cage size from Li_6PS_5I to Li_6PS_5Cl, despite the opposite trend in the lattice volume.

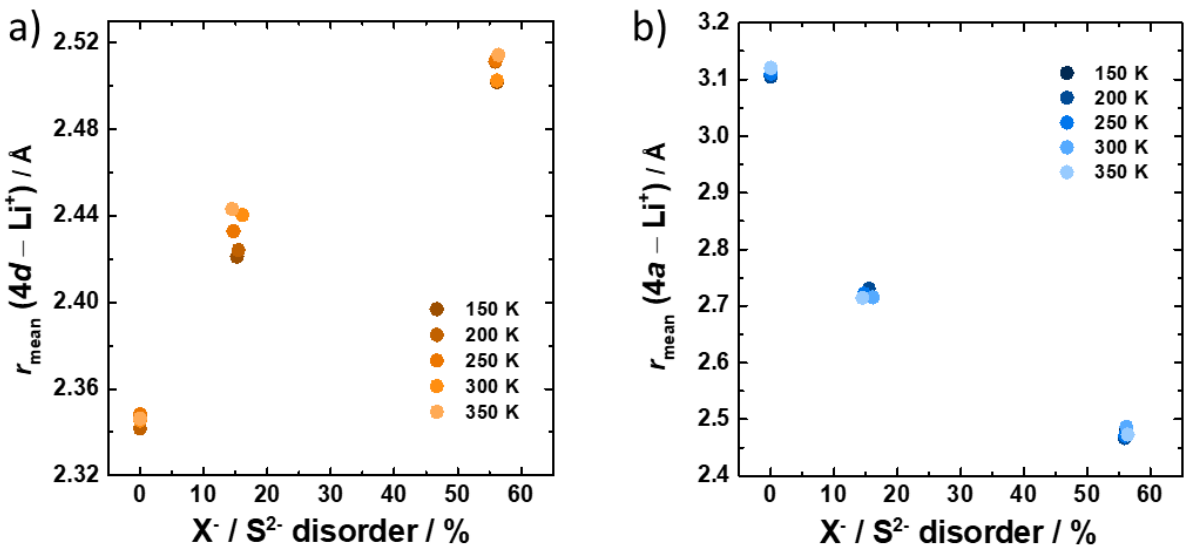

Figure 6: Weighted average distance r_{mean} of the Li^+ ions away from the center of the cage (i.e. nominal free sulfur position Wyckoff 4d) (a), and from the nominal halide position (Wyckoff 4a) (b) as a function of the anion site-disorder for all temperatures. With increasing disorder, less anionic charge is found within the cages and the cages are less contracted and extend towards the halide nominal position.

Diffusion pathways. In addition to the general trends in lithium-site occupancy discussed above, a more detailed analysis of the Li positions on the T2 and T5 sites in each system can help provide insight into the lithium diffusion pathways in these systems. The significance of the type 2 position was first noted by Deiseroth *et al.*,[38] who observed that this site must play a role in any continuous three-dimensional diffusion pathway through the argyrodite lattice. Figure 7 illustrates how each individual T2 site connects pairs of type 5 positions within the same cage, and pairs of face-sharing T2 sites connect type 5 sites in different cages, giving a contiguous network of face sharing tetrahedra. The T2 site can therefore be seen as an "intermediate" site situated along the paths considered as *intra*-cage and the *inter*-cage jumps in the conventional three-jump model.[39] When considering the role of the T2 site, we obtain a different classification of possible diffusion pathways through the argyrodite structure: motion within a cage is possible via T5 – T2 – T5 Li^+ motion (new *intra*-cage process), and motion between two cages is possible via T5 – T2 – T2 – T5 Li^+ motion (new *inter*-cage process).

Further analysis of the structures obtained from our neutron data reveals that increasing the temperature and increasing the radius of the halide in Li_6PS_5X both cause an increase in Li^+ polyhedral volumes, and in the areas of the shared-faces between adjacent Li^+ tetrahedra. To further quantify the changes in the relative positions of the T2 and T5 sites, we consider the T2–T5 distance (new *intra*-cage), T2–T2 distance (new *inter*-cage), T5–T5 distance within the

same cage (old *intra*-cage), and T5–T5 distance between adjacent cages (old *inter*-cage) (Supporting Information, Figure S5). We find that the distance between two different type 2 positions along the *inter*-cage jump is significantly smaller for *X* = Cl compared to *X* = Br, and therefore appears to be inversely correlated with the degree of anion disorder, in general agreement with the site–site distances predicted by molecular dynamics simulations.[42] This decrease in T2–T2 distance with increasing anion disorder is also consistent with the experimentally observed increase in Li^+ cage radius, which we attribute to the lower average negative charge of the Wyckoff 4*d* anionic center (*vide supra*). This analysis suggests that *inter*-cage jumps are more likely to happen for Li_6PS_5Cl compared to Li_6PS_5Br, as already theoretically suggested,[39] with this effect dependent on the degree of anion site-disorder, and the associated effect on the size of the Li^+ cages and correspondingly on the average T2–T2 distance.

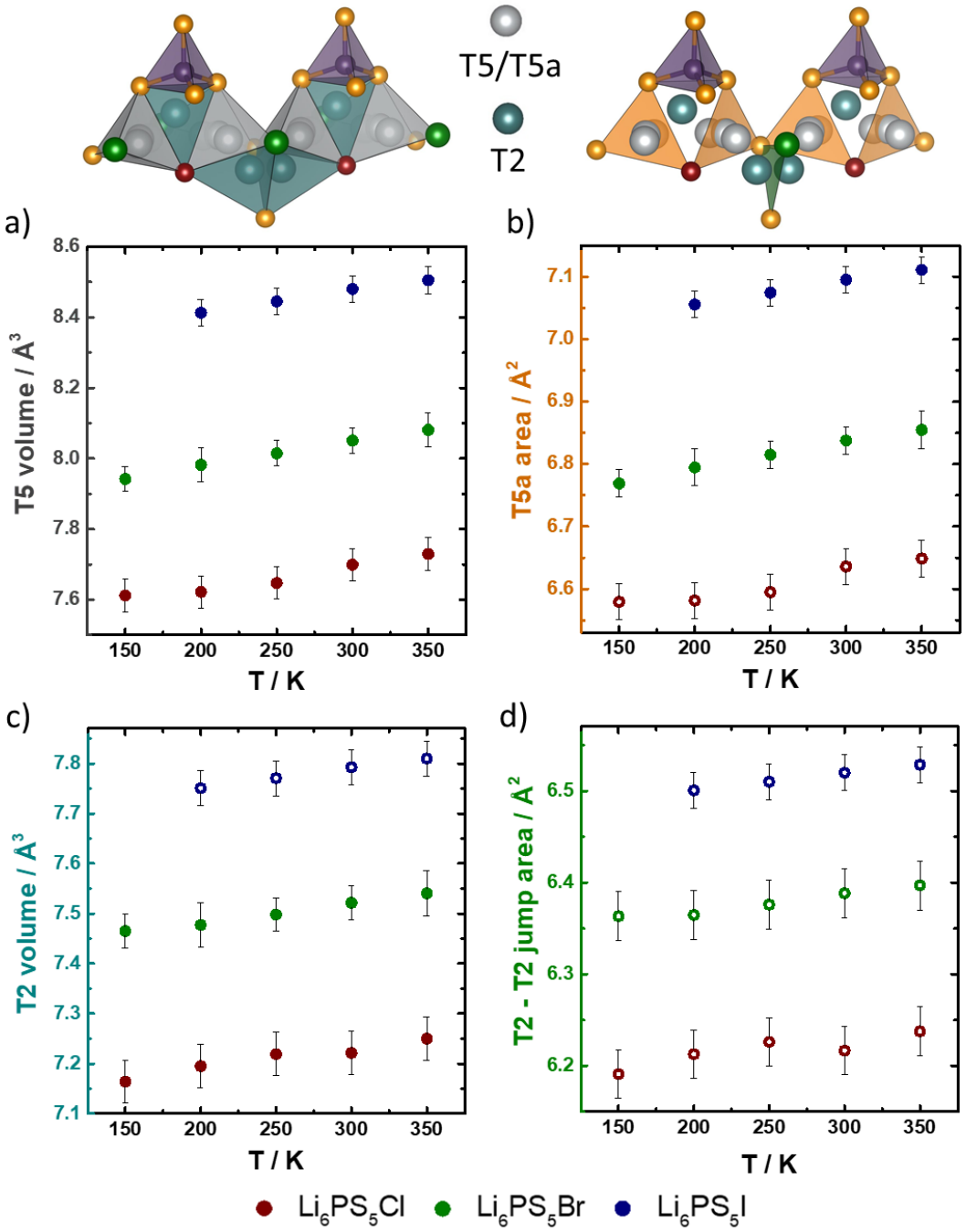

Figure 7: (a, c) changing polyhedral volumes and (b, d) areas along the Li^+ diffusion pathways with temperature. Closed symbols represent positions that are found occupied, and open symbols site in which no Li^+ was experimentally found. With increasing temperature, a broadening of the diffusion pathways by expanding Li^+ polyhedral volumes and transition areas can be found, likely facilitating easier ionic transport.

4. Discussion

The temperature-dependent neutron diffraction analysis of the Li^+ positions in Li_6PS_5X (X = Cl, Br, I), as described above, provides a precise description of the average Li^+ substructure in these lithium argyrodites as a function of the X^-/S^{2-} anionic site-disorder. Based on the observed changes in the lithium sublattice, a few conclusions may be drawn:

1) Based on the experimentally found lithium occupancy on the type 2 sites, the conduction pathways for the Li_6PS_5X argyrodites need to be reevaluated. Figure 8 shows the different site connectivity for Li^+. The model proposed by Wagemaker *et al.*[39] considers three different jumps, that feature the two so-far known positions type 5 and type 5a. However, direct *intra*- and *inter*-cage T5–T5 jumps are not possible via continuous face sharing T5-only pathways, therefore, long-range lithium diffusion involving type 5 sites only is improbable. Our results presented here suggest a key role is played by type 2 sites, and that, as already shown for the parent Ag-argyrodite,[18,19] type 2 sites take part both in ionic diffusion within the same lithium cluster (*intra*-cage) and in ionic diffusion between clusters (*inter*-cage), giving a much better connectivity of the lithium substructure (inserts in Figure 7), than when type 5 sites only are considered. These results are also supported by previous topological analyses of the conduction pathways via bond valence calculations.[40,44,45]
   Recently, in $Li_{6+x}Sb_{1-x}M_xS_5I$ (M = Si, Ge) Li^+ was found to partially occupy the T2 positions,[33] and it was suggested that the excess lithium stoichiometry $x(Li) > 6$ was the origin of this non-T5 site occupation. The results presented herein, however, show that even in Li_6PS_5Cl and Li_6PS_5Br, with nominal $x(Li) = 6$ stoichiometry, T2 positions are significantly occupied. Nevertheless, aliovalent substitution may lead to enhanced T2 occupation in structures such as Li_6PS_5I or Li_6SbS_5I where Li ions otherwise exclusively occupy T5 positions. The T2 position should therefore be considered in future theoretical and experimental analyses of the lithium distribution in all lithium argyrodites, including halide-free compositions, such as Li_7PS_6, or stoichiometries with $x(Li) < 6$, as a possible occupied site.
2) Increasing the degree of X^-/S^{2-} anion site disorder increases the halide occupancy of the Wyckoff 4*d* center, and gives a smaller average negative charge at this position. The correlation between increased X^-/S^{2-} disorder and the associated change in the lithium substructure suggests that a reduced magnitude average 4*d*-site charge may be the driving factor for the occupation of the T2 site. Experimentally, we have shown that increased anion disorder is correlated not only with increased lithium occupancy of the T2 sites, but also with an increase in the size of the Wyckoff 4*d*-centered Li^+ cages and an associated decrease

in the "inter-cage" T2–T2 jump distance. These correlations highlight the complex interplay between changes in anion distribution and the associated changes distribution of anionic charge—which becomes "inhomogeneous" across otherwise equivalent sites in anion-disordered systems—and changes in the site-distribution and relative positions of lithium ions.[42] Due to this complexity, we propose that a single model of lithium substructure cannot satisfactorily be applied to all lithium argyrodites, and that instead separate models are required for argyrodites with qualitatively different degrees of site-disorder:

(i) Structures with site-disorder close to 50% possess a statistical distribution of X^- and S^{2-} over the two anionic positions (Wyckoff 4*d* and 4*a*) resulting in a highly inhomogeneous charge distribution. In this case, models that consider well-defined Wyckoff 4*d*-centric Li^+ cages are likely an oversimplification. The close similarity of the average lithium distance from the nominal free sulfur and the halide position (*e.g.* 2.51 Å and 2.48 Å at 200 K for Li_6PS_5Cl, respectively) indicates a highly delocalized lithium density, where the lithium ions do not converge around one particular anionic center but are statistically distributed around both the halide and the free sulfur nominal positions.

(ii) Nevertheless, the idea of Li^+ cages is still effective in describing the lithium sub-lattice for structures with site-disorder closer to 0 % or 100 %, where the lithium ions appear to preferentially form cages around Wyckoff 4*d* (nominal free sulfur) and Wyckoff 4*a* (nominal halide) positions, respectively.[35,42] This consideration highlights that conceptual models that attempt to directly correlate higher degrees of X^-/S^{2-} anion exchange with enhanced lithium transport are incomplete. As noted elsewhere,[42] structures with 100 % exchange between S^{2-} and X^- anions would still give a homogenous anionic charge distributions, and are therefore expected to give poor long-range ionic mobility despite higher T2 occupancy. Indeed, this exact behavior is observed in molecular dynamics simulations, where the degree of X^-/S^{2-} site exchange can be manipulated freely.[39,42] Therefore, we expect that enhancements in the ionic transport can only be achieved by large anionic charge inhomogeneity stemming from site-disorder degrees close to 50 %. This model suggests that highest disorder in the Li^+ substructure will ultimately lead to fastest ionic transport.

3) Lithium has previously been assigned as partially occupying the T2 position in the $x(Li) > 6$ stoichiometry $Li_{6+x}Sb_{1-x}M_xS_5I$ (*M* = Si, Ge) argyrodites.[33] This observation prompted the suggestion that lithium occupation of these additional sites is driven by aliovalent

substitution and the commensurate increase in lithium stoichiometry. This analysis, however, is complicated by the progressive emergence of anion site-disorder that accompanies aliovalent substitution. It therefore remains an open question whether introducing additional Li^+ on the T2 site in aliovalently substituted systems drives an increase in anion disorder, or if switching on site-disorder—possibly as a direct result of the aliovalent substitution—leads to increased Li occupancy of T2 sites. At this stage it is only known that aliovalent substitution significantly affects the lithium substructure.[26,32,33] We note that, in addition to the T2 lithium positions found in this work, a fourth position, namely T4 (Figure 1), has been proposed as being partially occupied in anion disordered Li_6PS_5Cl, based on lithium distributions from molecular dynamics simulations.[42] As shown in Figure 8c, lithium diffusion via T4 would give even better connectivity between lithium positions throughout the argyrodite structure than a network comprising only T2 and T5 sites. While this site has not been detected in the compositions investigated here, type 4 positions are found to play a major role in the diffusion mechanism as a transient high-energy site in the excess lithium stoichiometry $x(Li) > 6$ argyrodite $Li_{6.15}M'_{1.5}S_6$ and the related oxysulfide $Li_{6.15}M'_{1.5}S_{5.4}O_{0.6}$ (M' = $Al_{0.1}Si_{0.9}$).[47,48] Therefore, conduction pathways including type 4 tetrahedral sites cannot be ruled out in argyrodite compositions when aliovalent substitution occurs.

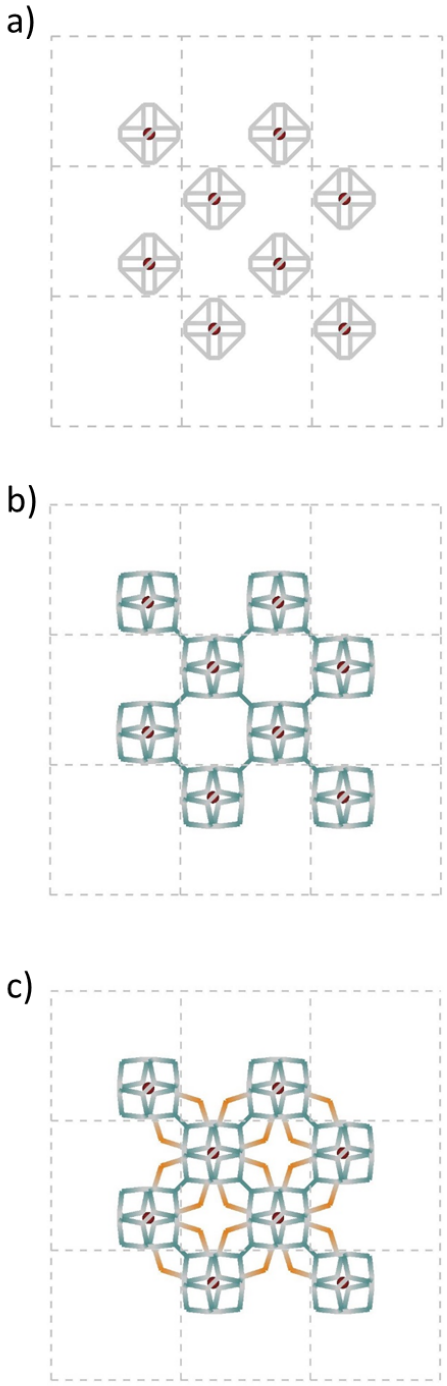

Figure 8: Representation of the Li^+ connectivity with (a) the T5 and T5a sites (grey) only, (b) including the experimentally found T2 position (tail) and a (c) topologically possible, so far unconfirmed, T4 site (orange). Diffusion trajectories involving T5 sites only form discontinuous face-sharing tetrahedral pathways.

5. Conclusion

We have performed a temperature-dependent neutron diffraction analysis of the Li^+ positions and site occupancies in the Li_6PS_5X (X = Cl, Br, I) argyrodites. This study has revealed the

correlation between X^{-}/S^{2-} anionic site-disorder and specific features in the lithium substructure has been revealed. From our analysis of the high-resolution diffraction data, we have identified new lithium positions, that have not been experimentally observed before for x(Li) = 6 lithium argyrodite stoichiometries, in agreement with previous computational predictions.[42] X^{-}/S^{2-} disorder can be considered to introduce charge-inhomogeneity into the anionic sublattice, which results in a more diffuse lithium density across the previously observed type 5 and type 5a, and newly assigned type 2 sites. The correlation between anion disorder, lithium redistribution, and enhanced lithium transport provides a possible explanation for the superior lithium-ion conductivities of anion-disordered versus anion-ordered argyrodites. In light of the observed lithium occupancy on additional sites, a new conduction pathway is proposed that provides a more complete description of the lithium diffusion mechanism in Li_6PS_5X argyrodites than previous mechanistic models. Our observations illustrate the utility of detailed structural studies in explaining composition–structure–transport relationships in this family of solid lithium-ion electrolytes, and we highlight the potential of future study of more complex lithium-argyrodite compositions; in particular, those involving aliovalent doping to achieve stoichiometries with more than six lithium atoms per formula unit. Ultimately, the general understanding of the crystallographic structure gained with this work provides a benchmark for future experimental and theoretical analyses of the argyrodite family.

Acknowledgments

The research was supported by the Deutsche Forschungsgemeinschaft (DFG) under grant number ZE 1010/4-1. This research used resources at the Spallation Neutron Source (IPTS-23414.1), operated by the Oak Ridge National Laboratory. B. J. M. acknowledges support from the Royal Society (UF130329 & URF\R\191006).

Supporting Information

Experimental neutron powder diffractograms for all explored temperatures and compositions are reported here. Additionally, tables with the constraints applied during Rietveld refinements, explored sites for lithium occupancy, the obtained crystallographic information files and Fourier maps are provided. The associated content also contains all the Li–Li distances as a function of temperature and composition.

References

(1) Janek, J.; Zeier, W. G. A Solid Future for Battery Development. *Nat. Energy* **2016**, *1*, 16141.

(2) Famprikis, T.; Canepa, P.; Dawson, J. A.; Islam, M. S.; Masquelier, C. Fundamentals of Inorganic Solid-State Electrolytes for Batteries. *Nat. Mater.* **2019**, *18*,1278–1291.

(3) Goodenough, J. B.; Park, K. S. The Li-Ion Rechargeable Battery: A Perspective. *J. Am. Chem. Soc.* **2013**, *135*, 1167–1176.

(4) Culver, S. P.; Koerver, R.; Krauskopf, T.; Zeier, W. G. Designing Ionic Conductors: The Interplay between Structural Phenomena and Interfaces in Thiophosphate-Based Solid-State Batteries. *Chem. Mater.* **2018**, *30*, 4179–4192.

(5) Ohno, S.; Koerver, R.; Dewald, G.; Rosenbach, C.; Titscher, P.; Steckermeier, D.; Kwade, A.; Janek, J.; Zeier, W. G. Observation of Chemomechanical Failure and the Influence of Cutoff Potentials in All-Solid-State Li-S Batteries. *Chem. Mater.* **2019**, *31*, 2930–2940.

(6) Dewald, G. F.; Ohno, S.; Kraft, M. A.; Koerver, R.; Till, P.; Vargas-Barbosa, N. M.; Janek, J.; Zeier, W. G. Experimental Assessment of the Practical Oxidative Stability of Lithium Thiophosphate Solid Electrolytes. *Chem. Mater.* **2019**, *31*, 8328–8337.

(7) Liang, J.; Wang, C.; Li, X.; Li, X.; Xia, W.; Li, R.; Huang, H.; Zhang, L.; Zhao, S.; Lu, S.; *et al.* Ultrastable Anode Interface Achieved by Fluorinating Electrolytes for All-Solid-State Li Metal Batteries. *ACS Energy Lett* **2020**, *5*, 1035–1043.

(8) Zhao, F.; Liang, J.; Yu, C.; Sun, Q.; Li, X.; Adair, K.; Wang, C.; Zhao, Y.; Zhang, S.; Li, W.; *et al.* A Versatile Sn-Substituted Argyrodite Sulfide Electrolyte for All-Solid-State Li Metal Batteries. *Adv. Energy Mater.* **2020**, *10*, 1903422.

(9) Kraft, M. A.; Culver, S. P.; Calderon, M.; Böcher, F.; Krauskopf, T.; Senyshyn, A.; Dietrich, C.; Zevalkink, A.; Janek, J.; Zeier, W. G. Influence of Lattice Polarizability on the Ionic Conductivity in the Lithium Superionic Argyrodites Li_6PS_5X (X = Cl, Br, I). *J. Am. Chem. Soc.* **2017**, *139*, 10909–10918.

(10) Yu, C.; Ganapathy, S.; De Klerk, N. J. J.; Roslon, I.; Van Eck, E. R. H.; Kentgens, A. P. M.; Wagemaker, M. Unravelling Li-Ion Transport from Picoseconds to Seconds: Bulk versus Interfaces in an Argyrodite Li_6PS_5Cl-Li_2S All-Solid-State Li-Ion Battery. *J. Am.*

Chem. Soc. **2016**, *138*, 11192–11201.

(11) Yu, C.; van Eijck, L.; Ganapathy, S.; Wagemaker, M. Synthesis, Structure and Electrochemical Performance of the Argyrodite Li_6PS_5Cl Solid Electrolyte for Li-Ion Solid State Batteries. *Electrochim. Acta* **2016**, *215*, 93–99.

(12) Wenzel, S.; Sedlmaier, S. J.; Dietrich, C.; Zeier, W. G.; Janek, J. Interfacial Reactivity and Interphase Growth of Argyrodite Solid Electrolytes at Lithium Metal Electrodes. *Solid State Ionics* **2018**, *318*, 102–112.

(13) Zhou, L.; Park, K. H.; Sun, X.; Lalère, F.; Adermann, T.; Hartmann, P.; Nazar, L. F. Solvent-Engineered Design of Argyrodite Li_6PS_5X (X = Cl, Br, I) Solid Electrolytes with High Ionic Conductivity. *ACS Energy Lett.* **2019**, *4*, 265–270.

(14) Epp, V.; Gün, Ö.; Deiseroth, H. J.; Wilkening, M. Highly Mobile Ions: Low-Temperature NMR Directly Probes Extremely Fast Li Hopping in Argyrodite-Type Li_6PS_5Br. *J. Phys. Chem. Lett.* **2013**, *4*, 2118–2123.

(15) Hanghofer, I.; Gadermaier, B.; Wilkening, H. M. R. Fast Rotational Dynamics in Argyrodite-Type Li_6PS_5X (X: Cl, Br, I) as Seen by ^{31}P Nuclear Magnetic Relaxation - On Cation-Anion Coupled Transport in Thiophosphates. *Chem. Mater.* **2019**, *31*, 4591–4597.

(16) Ganapathy, S.; Yu, C.; van Eck, E. R. H.; Wagemaker, M. Peeking across Grain Boundaries in a Solid-State Ionic Conductor. *ACS Energy Lett.* **2019**, *4*, 1092–1097.

(17) Deiseroth, H. J.; Kong, S. T.; Eckert, H.; Vannahme, J.; Reiner, C.; Zaiß, T.; Schlosser, M. Li_6PS_5X: A Class of Crystalline Li-Rich Solids with an Unusually High Li^+ Mobility. *Angew. Chemie - Int. Ed.* **2008**, *47*, 755–758.

(18) Boucher, F.; Evain, M.; Brec, R. Distribution and Ionic Diffusion Path of Silver in γ-Ag_8GeTe_6: A Temperature Dependent Anharmonic Single Crystal Structure Study. *Journal of Solid State Chemistry* **1993**, *107*, 332–346.

(19) Boucher, F.; Evain, M.; Brec, R. Single-Crystal Structure Determination of γ-Ag_8SiTe_6 and Powder X-Ray Study of Low-Temperature α and β Phases. *J. Solid State Chem.* **1992**, *100*, 341–355.

(20) Gągor, A.; Pietraszko, A.; Kaynts, D. Diffusion Paths Formation for Cu^+ Ions in Superionic Cu_6PS_5I Single Crystals Studied in Terms of Structural Phase Transition. *J. Solid State Chem.* **2005**, *178*, 3366–3375.

(21) Gagor, A.; Pietraszko, A.; Kaynts, D. Structural Aspects of Fast Copper Mobility in Cu_6PS_5Cl-The Best Solid Electrolyte from Cu_6PS_5X Series. *J. Solid State Chem.* **2008**, *181*, 777–782.

(22) Gaudin, E.; Boucher, F.; Petricek, V.; Taulelle, F.; Evain, M. Structures and Phase Transitions of the A_7PSe_6 (A = Ag, Cu) Argyrodite-Type Ionic Conductors. II. β- And γ-Cu_7PSe_6. *Acta Crystallogr. Sect. B* **2000**, *B56*, 402–408.

(23) Evain, M.; Gaudin, E.; Boucher, F.; Petricek, V.; Taulelle, F. Structures and Phase Transitions of the A_7PSe_6 (A = Ag, Cu) Argyrodite-Type Ionic Conductors. I. Ag_7PSe_6. *Acta Crystallogr. Sect. B Struct. Sci.* **1998**, *54*, 376–383.

(24) Bernges, T.; Culver, S. P.; Minafra, N.; Koerver, R.; Zeier, W. G. Competing Structural In Fl Uences in the Li Superionic Conducting Argyrodites $Li_6PS_{5-x}Se_xBr$ ($0 \leq x \leq 1$) upon Se Substitution. *Inorg. Chem.* **2018**, *57*, 13920–13928.

(25) Adeli, P.; Bazak, J. D.; Park, K. H.; Kochetkov, I.; Huq, A.; Goward, G. R.; Nazar, L. F. Boosting Solid-State Diffusivity and Conductivity in Lithium Superionic Argyrodites by Halide Substitution. *Angew. Chemie - Int. Ed.* **2019**, *58*, 8681–8686.

(26) Ohno, S.; Helm, B.; Fuchs, T.; Dewald, G.; Kraft, M. A.; Culver, S. P.; Senyshyn, A.; Zeier, W. G. Further Evidence for Energy Landscape Flattening in the Superionic Argyrodites $Li_{6+x}P_{1-x}M_xS_5I$ (M = Si, Ge, Sn). *Chem. Mater.* **2019**, *31*, 4936–4944.

(27) Minafra, N.; Culver, S. P.; Krauskopf, T.; Senyshyn, A.; Zeier, W. G. Effect of Si Substitution on the Structural and Transport Properties of Superionic Li-Argyrodites. *J. Mater. Chem. A* **2018**, *6*, 645–651.

(28) Schlem, R.; Ghidiu, M.; Culver, S. P.; Hansen, A. L.; Zeier, W. G. Changing the Static and Dynamic Lattice Effects for the Improvement of the Ionic Transport Properties within the Argyrodite $Li_6PS_{5-x}Se_xI$. *ACS Appl. Energy Mater.* **2019**, *3*, 9–18.

(29) Feng, X.; Chien, P.; Wang, Y.; Patel, S.; Wang, P.; Liu, H.; Immediato-scuotto, M.; Hu, Y. Enhanced Ion Conduction by Enforcing Structural Disorder in Li-Deficient Argyrodites $Li_{6-x}PS_{5-x}Cl_{1+x}$. *Energy Storage Mater.* **2020**, *30*, 67–73.

(30) Yu, C.; Li, Y.; Willans, M. J.; Zhao, Y.; Adair, K. R.; Zhao, F.; Li, W.; Deng, S.; Liang, J.; Banis, M. N.; *et al.* Superionic Conductivity in Lithium Argyrodite Solid-State Electrolyte by Controlled Cl-Doping. *Nano Energy* **2019**, *69*, 104396.

(31) Yu, C.; Li, Y.; Li, W.; Adair, K. R.; Zhao, F.; Willans, M.; Liang, J.; Zhao, Y.; Wang,

C.; Deng, S.; *et al.* Enabling Ultrafast Ionic Conductivity in Br-Based Lithium Argyrodite Electrolytes for Solid-State Batteries with Different Anodes. *Energy Storage Mater.* **2020**, *30*, 238–249.

(32) Kraft, M. A.; Ohno, S.; Zinkevich, T.; Koerver, R.; Culver, S. P.; Fuchs, T.; Senyshyn, A.; Indris, S.; Morgan, B. J.; Zeier, W. G. Inducing High Ionic Conductivity in the Lithium Superionic Argyrodites $Li_{6+x}P_{1-x}Ge_xS_5I$ for All-Solid-State Batteries. *J. Am. Chem. Soc.* **2018**, *140*, 16330–16339.

(33) Zhou, L.; Assoud, A.; Zhang, Q.; Wu, X.; Nazar, L. F. A New Family of Argyrodite Thioantimonate Lithium Superionic Conductors. *J. Am. Chem. Soc.* **2019,** *141*, 19002–19013.

(34) Kong, S. T.; Deiseroth, H. J.; Reiner, C.; Gün, Ö.; Neumann, E.; Ritter, C.; Zahn, D. Lithium Argyrodites with Phosphorus and Arsenic: Order and Disorder of Lithium Atoms, Crystal Chemistry, and Phase Transitions. *Chem. - A Eur. J.* **2010**, *16*, 2198–2206.

(35) Rao, R. P.; Sharma, N.; Peterson, V. K.; Adams, S. Formation and Conductivity Studies of Lithium Argyrodite Solid Electrolytes Using In-Situ Neutron Diffraction. *Solid State Ionics* **2013**, *230*, 72–76.

(36) Gautam, A.; Sadowski, M.; Prinz, N.; Eickhoff, H.; Minafra, N.; Ghidiu, M.; Culver, S. P.; Albe, K.; Fässler, T. F.; Zobel, M.; *et al.* Rapid Crystallization and Kinetic Freezing of Site-Disorder in the Lithium Superionic Argyrodite Li_6PS_5Br. *Chem. Mater.* **2019**, *31*, 10178–10185.

(37) Stamminger, A. R.; Ziebarth, B.; Mrovec, M.; Hammerschmidt, T.; Drautz, R. Ionic Conductivity and Its Dependence on Structural Disorder in Halogenated Argyrodites Li_6PS_5X (X = Br, Cl, I). *Chem. Mater.* **2019**, *31*, 8673–8678.

(38) Deiseroth, H. J.; Maier, J.; Weichert, K.; Nickel, V.; Kong, S. T.; Reiner, C. Li_7PS_6 and Li_6PS_5X (X: Cl, Br, I): Possible Three-Dimensional Diffusion Pathways for Lithium Ions and Temperature Dependence of the Ionic Conductivity by Impedance Measurements. *Zeitschrift fur Anorg. und Allg. Chemie* **2011**, *637*, 1287–1294.

(39) De Klerk, N. J. J.; Rosłoń, I.; Wagemaker, M. Diffusion Mechanism of Li Argyrodite Solid Electrolytes for Li-Ion Batteries and Prediction of Optimized Halogen Doping: The Effect of Li Vacancies, Halogens, and Halogen Disorder. *Chem. Mater.* **2016**, *28*, 7955–7963.

(40) Rayavarapu, P. R.; Sharma, N.; Peterson, V. K.; Adams, S. Variation in Structure and Li^+-Ion Migration in Argyrodite-Type Li_6PS_5X (X = Cl, Br, I) Solid Electrolytes. *J. Solid State Electrochem.* **2012**, *16*, 1807–1813.

(41) Wang, P.; Liu, H.; Patel, S.; Feng, X.; Chien, P.; Wang, Y.; Hu, Y. Fast Ion Conduction and Its Origin in $Li_{6-x}PS_{5-x}Br_{1+x}$. *Chem. Mater.* **2020**, *32*, 3833–3840.

(42) Morgan, B. J. Mechanistic Origin of Superionic Lithium Conduction in Substitutionally Disordered Li_6PS_5X Argyrodites. *ChemRxiv* **2020**, Preprint. https://doi.org/10.26434/chemrxiv.12349703.v1

(43) Hanghofer, I.; Brinek, M.; Eisbacher, S. L.; Bitschnau, B.; Volck, M.; Hennige, V.; Hanzu, I.; Rettenwander, D.; Wilkening, H. M. R. Substitutional Disorder: Structure and Ion Dynamics of the Argyrodites Li_6PS_5Cl, Li_6PS_5Br and Li_6PS_5I. *Phys. Chem. Chem. Phys.* **2019**, *21*, 8489–8507.

(44) Chen, H. M.; Maohua, C.; Adams, S. Stability and Ionic Mobility in Argyrodite-Related Lithium-Ion Solid Electrolytes. *Phys. Chem. Chem. Phys.* **2015**, *17*, 16494–16506.

(45) Rao, R. P.; Adams, S. Studies of Lithium Argyrodite Solid Electrolytes for All-Solid-State Batteries. *Phys. Status Solidi Appl. Mater. Sci.* **2011**, *208*, 1804–1807.

(46) Pecher, O.; Kong, S. T.; Goebel, T.; Nickel, V.; Weichert, K.; Reiner, C.; Deiseroth, H. J.; Maier, J.; Haarmann, F.; Zahn, D. Atomistic Characterisation of Li^+ Mobility and Conductivity in $Li_{7-x}PS_{6-x}I_x$ Argyrodites from Molecular Dynamics Simulations, Solid-State NMR, and Impedance Spectroscopy. *Chem. - A Eur. J.* **2010**, *16*, 8349–8354.

(47) Huang, W.; Yoshino, K.; Hori, S.; Suzuki, K.; Yonemura, M.; Hirayama, M.; Kanno, R. Superionic Lithium Conductor with a Cubic Argyrodite-Type Structure in the Li–Al–Si–S System. *J. Solid State Chem.* **2019**, *270*, 487–492.

(48) Huang, W.; Cheng, L.; Hori, S.; Suzuki, K.; Yonemura, M.; Hirayamaa, M.; Kanno, R. Ionic Conduction Mechanism of a Lithium Superionic Argyrodite in the Li-Al-Si-S-O System. *Mater. Adv.,* **2020**, *Advance Ar*. https://doi.org/10.1039/D0MA00115E.

(49) Calder, S.; An, K.; Boehler, R.; Dela Cruz, C. R.; Frontzek, M. D.; Guthrie, M.; Haberl, B.; Huq, A.; Kimber, S. A. J.; Liu, J.; et al. A Suite-Level Review of the Neutron Powder Diffraction Instruments at Oak Ridge National Laboratory. *Rev. Sci. Instrum.* **2018**, *89*, 092701.

(50) Huq, A.; Hodges, J. P.; Gourdon, O.; Heroux, L. Powgen: A Third-Generation

Highresolution High-Throughput Powder Diffraction Instrument at the Spallation Neutron Source. *Z. Kristallogr. Proc.* **2011**, *1*, 127–135.

(51) Huq, A.; Kirkham, M.; Peterson, P. F.; Hodges, J. P.; Whitfield, P. S.; Page, K.; Hugle, T.; Iverson, E. B.; Parizzia, A.; Rennichb, G. POWGEN: Rebuild of a Third-Generation Powder Diffractometer at the Spallation Neutron Source. *J. Appl. Crystallogr.* **2019**, *52*, 1189–1201.

(52) Coelho, A. A. TOPAS-Academic. Brisbane, Australia 2007.

(53) Shannon, R. D. Revised Effective Ionic Radii in Halides and Chalcogenides. *Acta Cryst.* **1976**, *A32*, 751–767.

TOC

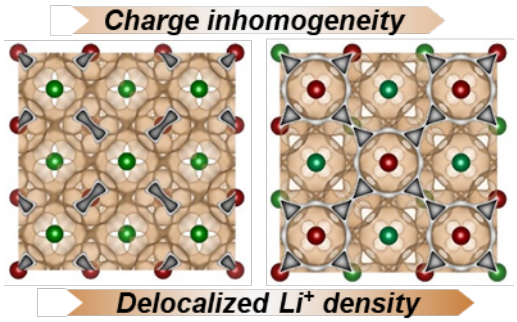

Synopsis

In this study, we performed Rietveld refinements against temperature-dependent neutron diffraction data to better understand the structural properties that govern Li^+ motion in the Li_6PS_5X argyrodites. Our analysis reveals an additional lithium position and different conduction pathways than previously proposed. The study of Li^+ radial distributions shows that greater anionic charge inhomogeneity leads to more delocalized lithium density. Finally, the herein found correlations provide a possible explanation for the enhanced lithium transport in anion-disordered argyrodites.